MRS Communications (2017), 7, 563–569
© Materials Research Society, 2017
doi:10.1557/mrc.2017.55

MRS Communications

Research Letter

Economical Fe-doped Ta_2O_5 electrocatalyst toward efficient oxygen evolution: a combined experimental and first-principles study

Aihong Liu, School of Materials and Metallurgy, Hubei Polytechnic University, Huangshi 435003, Hubei Province, People's Republic of China
Zhe Chen, Xiangxia Wei, Wen Xiao, and **Jun Ding,** Department of Materials Science and Engineering, National University of Singapore, Singapore 117575, Singapore

Address all correspondence to Jun Ding at **msedingj@nus.edu.sg**

(Received 12 January 2017; accepted 6 July 2017)

Abstract

A non-precious metal catalytic system of Fe-doped Ta_2O_5 is developed by pulsed laser deposition toward efficient oxygen evolution reaction (OER). The optimal Fe concentration is determined to be 5 at.% for optimized OER activity via a series of electrochemical characterizations. The 5 at.% Fe-doped Ta_2O_5 nanolayer possesses a low onset overpotential of 0.22 V, an overpotential of 0.38 V at 10 mA/cm^2 and a Tafel slope of 54 mV/dec. Comprehensive first-principles calculations attribute the enhanced OER activity to the substitutional Fe_{Ta} dopants, which generate a new active OER site on surface and simultaneously accelerate electron transfer over oxygens.

Introduction

To meet the challenges of energy crisis and global warming, efficient and clean utilization of renewable energy sources, especially solar energy, is a necessity.[1–4] In addition to solar cell, solar-to-fuel and solar-to-hydrogen conversion, such as photocatalytic CO_2 reduction or water splitting, have recently attracted enormous interests for producing energy directly from sunlight and simultaneously storing the energy in the form of chemical fuels.[2,5] However, the overpotential induced by the anodic oxygen evolution reaction (OER) is usually much higher than that of the cathodic reaction (e.g., hydrogen evolution reaction) and limits the overall efficiency of energy conversion. It points out the prime importance of accelerating the sluggish OER.[6–11] Moreover, rapid OER also ensures the high efficiency of water electrolysis and rechargeable metal-air batteries, further emphasizing the urgency of designing high-performance OER catalysts.[12–15] IrO_2 or RuO_2 are conventional OER catalysts, which are unfortunately not possible for large-scale applications due to the high cost and scarcity.[16–19] As a result, searching for earth-abundant alternatives with high OER activity to replace the previous-metal catalysts forms a hot topic.

Transition metal compounds, particularly oxides/hydroxides of Fe, Co, Ni, Ta, Mn, and Cu as well as their mixtures, have been reported to be highly active in OER catalysis.[12,20–22] Therein, the OER catalysts involving element Fe attract tremendous attention owing to the high activity. Burke et al. report that the composition of Fe in Co–Fe (oxy)hydroxide is critical for optimizing the OER activity.[23] Moreover, Burke et al.[20] also compare the activities of various mixed metal (oxy)hydroxide and illustrate the high OER performance of the catalysts with Fe elements. Friebel et al.[24] identify the Fe sites in (Ni,Fe)OOH to be highly active for OER through a combined experimental and first-principles study. Görlin et al.[25] further propose that metal redox states in Ni–Fe oxide largely affect the OER dynamics. The above findings indicate the effective role of Fe to enhance the OER activity of various transition metal oxides/hydroxides, even though pure Fe hydroxides are typically poor in OER catalysis.[26] Recently, we have successfully developed a new OER catalyst of Ta_2O_5 nanolayer. It exhibits OER activity comparable with RuO_2 and IrO_2 and serves as a promising candidate of economical catalyst.[12] Considering the interesting feature of Fe for enhancing the OER activity of transition metal oxides, it is worthwhile further incorporating Fe into Ta_2O_5 matrix and developing an Fe-doped Ta_2O_5 nanolayer as a conspicuously new and economical catalytic system toward OER.

Herein, we combine experimental and first-principles study to design a novel economical catalytic system of Fe-doped Ta_2O_5 toward efficient oxygen evaluation. A series of Fe-doped Ta_2O_5 nanolayer catalysts with different Fe concentrations have been synthesized by pulsed laser deposition (PLD). We show that the Fe dopants can enhance the OER activity of Ta_2O_5 and obtain the optimal amount of Fe concentration via systematic electrochemical measurements. The best Fe-doped Ta_2O_5 (5 at.% Fe) OER catalyst exhibits a low onset overpotential of 0.22 V, an overpotential of 0.38 V at 10 mA/cm^2 and a small Tafel slope of 54 mV/dec. Moreover, first-principles simulation reveals that Fe dopants generate new additional active OER sites, which are responsible for the

https://doi.org/10.1557/mrc.2017.55 Published online by Cambridge University Press

enhanced OER activity. Last but not the least, we also investigate the effect of Fe dopants on the electronic property of Fe-doped Ta_2O_5 by first-principles approach and discuss the positive correlation between electron transfer efficiency and the OER catalytic performance. Our findings enrich the applications of the earth-abundant Fe element for enhancing the OER activity of transition metal oxides and pave the way for future development of economical catalysts toward OER.

Experimental

Deposition of Fe-doped Ta_2O_5 nanolayer

Fe-doped Ta_2O_5 nanolayers on carbon cloth were synthesized by PLD at a temperature of 550 °C under high oxygen partial pressure of 20 mTorr as in our previous work.[12] A KrF excimer laser was utilized with laser wavelength of 248 nm, energy density of 1.8 J/cm^2, and frequency of 5 Hz. The Fe concentration was varied from 0 to 10 at.% by using Fe-doped Ta_2O_5 targets of pure Ta_2O_5 (0 at.%), $Fe_{0.04}Ta_{1.92}O_5$ (2 at.%), $Fe_{0.1}Ta_{1.9}O_5$ (5 at.%), and $Fe_{0.2}Ta_{1.8}O_5$ (10 at.%). The same PLD conditions were applied for preparing α-Fe_2O_3 nanolayer using pure α-Fe_2O_3 target. The targets were prepared by mixing appropriate amount of fine Ta_2O_5 and α-Fe_2O_3 powder in a clean alumina mortar, followed by pressing and finally sintering in air at 1000 °C for 24 h. PLD is able to control the mass of deposition precisely via deterministic control of deposition parameters.

Materials characterizations

Field-emission scanning electron microscopy (FESEM; Zeiss Supra 40) was used to image the samples. Transmission electron microscopy (TEM; JEOL-2010 at 300 kV) was employed to take side-view high-resolution TEM (HRTEM) images of Fe-doped Ta_2O_5 nanolayers. The bonding characteristics and chemical states of the samples were studied by x-ray photoelectron spectroscopy (XPS; Kratos Analytical, Axis Ultra DLD). X-ray was generated by a monochromatic Al Kα source operating at 1486.7 eV. The charging effect was corrected by calibrating the C 1*s* photoelectron peak at 284.6 eV as an internal standard.

Electrochemical measurements

A VMP3 electrochemical workstation (Bio-logic Inc.) was used to perform electrochemical measurements. A three-electrode setup with reference electrode of Hg/HgO (1 M KOH), counter electrode of platinum and electrolyte of 1 M KOH solution was adopted for all measurements. The Fe-doped Ta_2O_5 nanolayer on carbon cloth samples were directly used as working electrodes. The size of the working electrode is kept at 1 × 1 cm^2. All linear sweep voltammetry (LSV) polarization curves were measured at a scan rate of 10 mV/s at room temperature with iR correction. The potential calibration with respect to the reversible hydrogen electrode (RHE) was performed using Nernst equation $E_{RHE} = E_{Hg/HgO} + 0.059 \times pH + E^0_{Hg/HgO}$, where pH = 13.7 and $E^0_{Hg/HgO} = 0.098$ V at 25 °C.

Results and discussion

Fe-doped Ta_2O_5 nanolayer samples of different Fe concentrations were deposited by PLD on carbon cloth as seen in Fig. 1(a) and the "Experimental" section. The carbon cloth with Fe-doped Ta_2O_5 nanolayer was then directly used as the working electrode for electrochemical measurement of OER. Notably, our previous work revealed that only the oxygen-rich (200) surface of Ta_2O_5 was active in OER catalysis, so this work employed identical deposition conditions to produce the (200) surface of Ta_2O_5 matrix.[12] Figure 1(b) shows the side-view HRTEM image of a typical Fe-doped Ta_2O_5 nanolayer (5 at.% Fe) of ~5 nm in thickness. The lattice spacing parallel to the surface is measured to be ~0.31 nm, which is in good agreement with that of the (200) surface of Ta_2O_5 (ICCD-JCPDS 25-0922).[12] It indicates that (200) surface of the Ta_2O_5 matrix forms by controlling the PLD parameters. In addition, (200) peak dominates in the XRD spectrum (Supplementary material: Fig. S1) for the 5 at.% Fe-doped Ta_2O_5 sample, indicating a (200)-textured crystal phase of Ta_2O_5. Furthermore, XPS spectra of Ta 4*f* and Fe 2*p* orbitals are shown to analyze the elemental information of the product as seen in Figs. 1(c) and 1(d). Ta $4f_{7/2}$ and $4f_{5/2}$ peaks are well fitted with Gaussian distribution centered at 26.50 and 28.42 eV respectively as shown in Fig. 1(c). The two peaks exhibit an energy separation of 1.92 eV suggesting that the Ta_2O_5 matrix processes strong Ta–O bonds with high quality.[27] Moreover, Fig. 1(d) illustrates the XPS spectrum of Fe 2*p* orbital, in which the two satellite peaks accompanying to $2p_{1/2}$ and $2p_{3/2}$ peaks are clearly seen. The satellite peak position beside the Fe $2p_{3/2}$ peak is ~719.0 eV, which is ascribed to Fe 3*d*–O 2*p* hybridization and suggests that Fe is fully oxidized to Fe^{3+} in Ta_2O_5 nanolayer.[28] It is because the sample is deposited under high oxygen partial pressure to induce the oxygen-rich (200) surface of Ta_2O_5 as described in the "Experimental" section. The above materials characterizations confirm that thin (~5 nm) Fe-doped Ta_2O_5 nanolayer with (200) surface are successfully fabricated for further electrochemical characterizations.

To investigate the effect of Fe dopants on the OER catalytic activity of Ta_2O_5 system, electrochemical measurements of OER were performed for pure Ta_2O_5, Fe-doped Ta_2O_5 and pure α-Fe_2O_3 samples. Figure 2(a) demonstrates the LSV polarization curves and depicts that the current density increases from ~74 to 109 mA/cm^2 at applied potential $U = 1.73$ V (overpotential $\eta = 0.5$ V) with increasing Fe concentration from 0 to 5 at.%. It indicates that Fe dopants can largely enhance the OER current density of Ta_2O_5 system by ~47%. Interestingly, when the Fe concentration further increases to 10 at.%, the current density at $\eta = 0.5$ V drops to 78.2 mA/cm^2. The trend suggests an optimal Fe concentration of 5 at.% for maximum OER activity. The drop of activity as a result of the overdoping of Fe can be because iron oxide itself has poor OER activity and the overdoped Fe may form iron oxide that decreases the amount of active OER surface sites in Ta_2O_5 system.[26] Furthermore, the

https://doi.org/10.1557/mrc.2017.55 Published online by Cambridge University Press

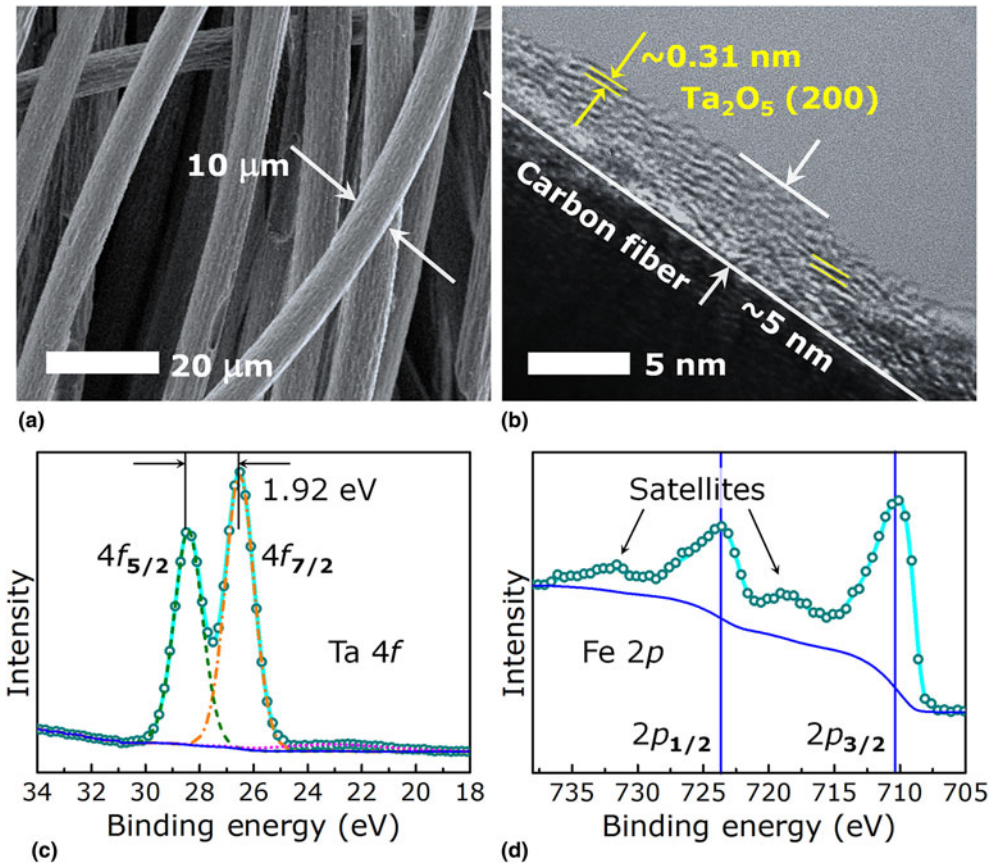


Figure 1. (a) SEM images of the carbon cloth composed of carbon fibers with diameter of 10 μm. (b) Side-view HRTEM image of the 5 nm Fe-doped Ta_2O_5 (5 at.% Fe) on carbon fiber. (c, d) XPS spectra of Ta 4*f* and Fe 2*p* orbitals of the 5 at.% Fe-doped Ta_2O_5 sample.

LSV polarization curve for pure α-Fe_2O_3 possesses extremely low current density. It confirms that the pure α-Fe_2O_3 is inactive in OER catalysis. Therefore, Fe dopants need to be incorporated into the Ta_2O_5 matrix for enhancing the OER activity of Fe-doped Ta_2O_5 system and overdoping of Fe deteriorates the OER performance. Figure 2(b) summarizes the onset overpotential and overpotential at 10 mA/cm^2 as a function of Fe concentration. The 5 at.% Fe-doped Ta_2O_5 possesses the best OER activity with a smallest onset overpotential of 0.22 V and an overpotential at 10 mA/cm^2 of 0.38 V. Figure 2(c) shows the Tafel plots derived from the LSV polarizations curves of the Fe-doped Ta_2O_5 samples in Fig. 2(a). The trend of Tafel slope as a function of Fe concentration [Fig. 2(d)] is in alignment with that of the overpotential [Fig. 2(c)]. The 5 at.% Fe-doped Ta_2O_5 sample has a small Tafel slope of 54 mV/dec, indicating a rapid kinetic OER process. The above trends have been confirmed by repeating the synthesis and measurements to ensure reproducibility. As a result, the electrochemical characterizations affirm that Fe dopants of suitable concentration effectively enhance the OER performance of the Fe-doped Ta_2O_5 system.

To confirm the role of Fe dopants in enhancing the OER catalytic activity, acid treatment was further performed on pure and 5 at.% Fe-doped Ta_2O_5 samples by immersing them in 10 mM HCl solution under sonication for 10 min. The acid-treated samples were then washed with water and dried in 20 mT O_2 gas at 300 °C for 30 min to heal the crystallinity. LSV polarization curves were measured and compared for the samples with and without acid treatment. Figure 2(e) shows that the as-prepared and acid-treated pure Ta_2O_5 samples have close OER catalytic activity. It indicates that the Ta_2O_5 matrix is chemically stable and inert in acid. In sharp contrast, the acid-treated 5 at.% Fe-doped Ta_2O_5 sample possesses much lower OER catalytic activity than that of the as-prepared sample. It can be because Fe–O bonds are less robust than Ta–O bonds in acid and the acid-treated sample losses Fe dopants in the surface region when being sonicated in acid. Therefore, Fe dopants are crucial for enhancing the OER catalytic activity of the Ta_2O_5 system.

To understand the mechanism of the enhanced the OER activity, extensive first-principles calculations are performed based on density functional theory (DFT). In this work, the orthorhombic λ-Ta_2O_5 is adopted as seen in Fig. 3(a) to study the Fe dopants in bulk and on surface of Ta_2O_5.[12,29] As Fe is fully oxidized to Fe^{3+} suggested by the XPS analysis

https://doi.org/10.1557/mrc.2017.55 Published online by Cambridge University Press

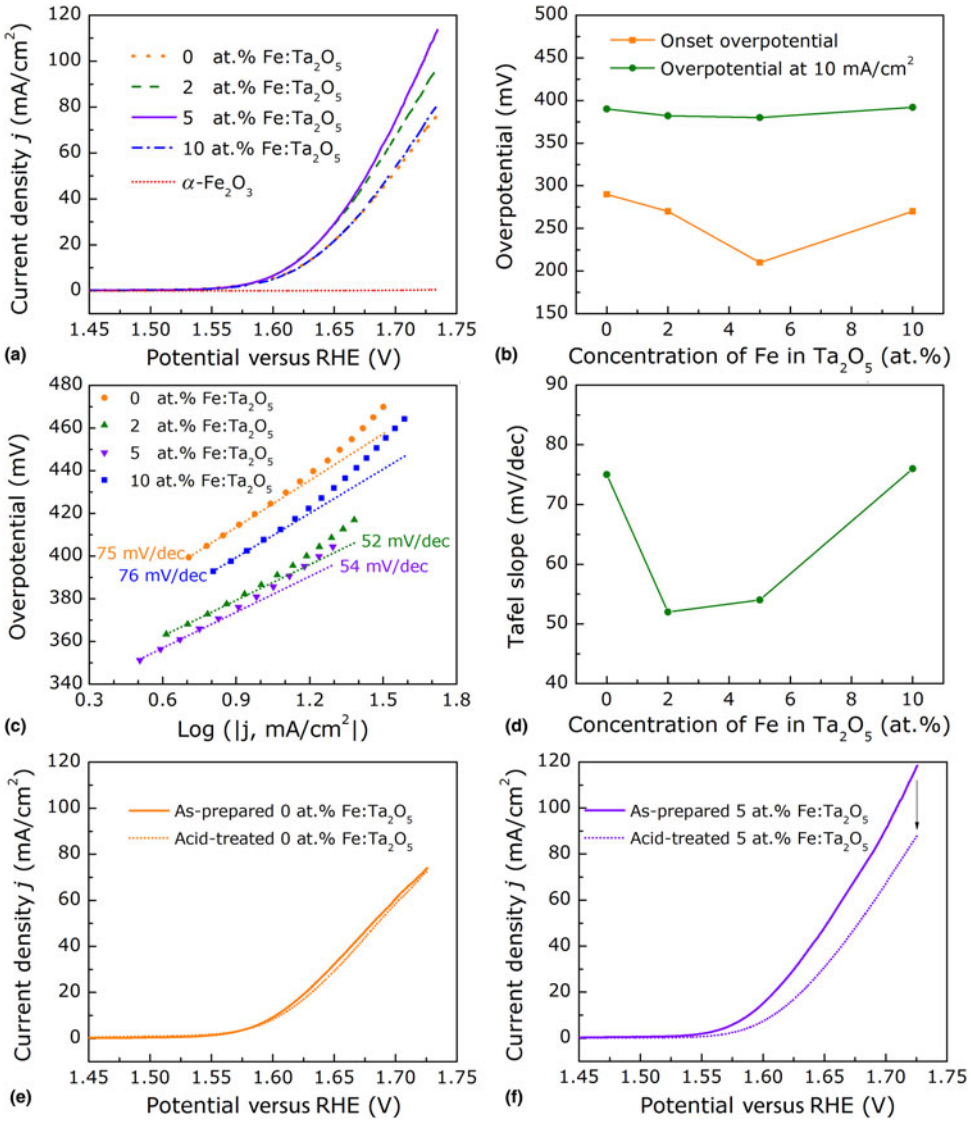


Figure 2. (a) OER LSV polarization curves of Fe-doped Ta_2O_5 with Fe concentration varying from 0 to 10 at.% in 1 M KOH at a scan rate of 10 mV/s. The LSV polarization curve for pure α-Fe_2O_3 is also shown for comparison. The iR loss from solution resistance is compensated via voltage correction. (b) Onset overpotential and overpotential at 10 mA/cm^2 as a function of Fe concentration in Ta_2O_5. (c) The corresponding Tafel plots derived from (a) for the Fe-doped Ta_2O_5 samples. (d) Tafel slope as a function of Fe concentration in Ta_2O_5. Onset overpotentials were determined based on the beginning of linear regime in the Tafel plot (Supplementary material: Fig. S2). (e) OER LSV polarization curves of the pure Ta_2O_5 sample with (solid line) and without (dotted line) acid treatment. (f) OER LSV polarization curves of the 5 at.% Fe-doped Ta_2O_5 sample with (solid line) and without (dotted line) acid treatment.

in Fig. 1(d), we focus on Fe substituted Ta (Fe_{Ta}) dopant with a high oxygen coordination number of six. In addition, spin-polarized calculations (Supplementary material: Fig. S3) reveals that there could be ferromagnetic coupling between Fe_{Ta} dopants in Ta_2O_5 matrix due to Fe 3*d*–O 2*p* hybridization, in good agreement with the XPS analysis [Fig. 1(d)] and SQUID measurement (Supplementary material: Fig. S3). It implies that substitutional Fe_{Ta} dopants dominate in the Ta_2O_5 system.

In the (200)-surface-exposed Ta_2O_5 nanolayer, there are two possible positions for Fe_{Ta} dopants, which are in bulk and on (200) surface as shown in Figs. 3(b) and 3(c), respectively. The formation energies of Fe_{Ta} dopants at the two positions are firstly calculated and compared as a function of chemical potential of oxygen [Fig. 3(d) and Supplementary material: Calculation methods]. It can be seen that the formation energies of the substitutional Fe_{Ta} decreases with increasing chemical potential of oxygen for both atomic positions. In oxygen-rich condition, the formation energies of Fe_{Ta} dopant in bulk and on (200) surface of Ta_2O_5 are as low as −2.0 and −2.7 eV, respectively. It suggests that Fe is favorable to substitute Ta when growing the Fe-doped Ta_2O_5 nanolayer under high oxygen partial pressure. Notably, the Fe-doped Ta_2O_5 samples are fabricated under high oxygen partial pressure, which thus

https://doi.org/10.1557/mrc.2017.55 Published online by Cambridge University Press

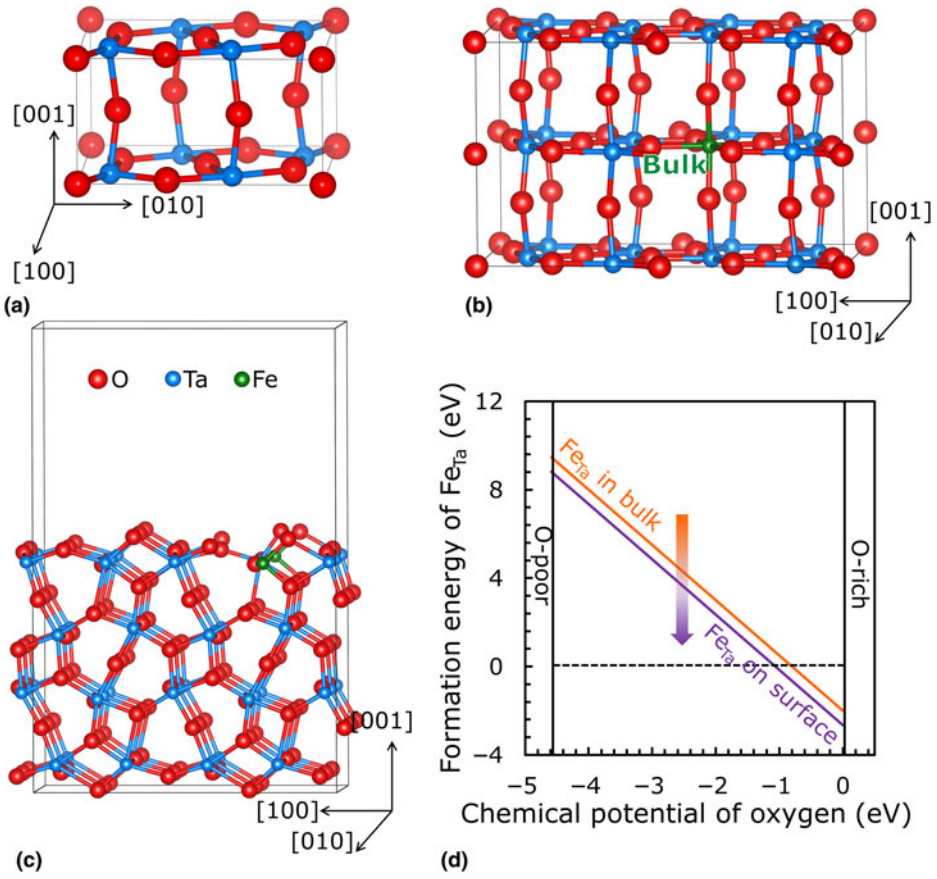


Figure 3. (a) Unit cell model of λ-Ta_2O_5 structure. (b) Atomic model of substitutional Fe dopant in bulk Ta_2O_5. (c) Atomic model of substitutional Fe dopant on the (200) surface of Ta_2O_5. (d) Formation energy of Fe substituted Ta (Fe_{Ta}) as a function of chemical potential of oxygen.

benefit the formation of substitutional Fe_{Ta} in Ta_2O_5 matrix. Moreover, the formation energy of Fe_{Ta} on the (200) surface is always 0.7 eV lower than that of Fe_{Ta} in bulk Ta_2O_5, indicating that Fe is more favorable to substitute Ta on surface than in bulk. As the catalytic kinetics and activity are mainly determined by the interactions between intermediates and surface, the Fe_{Ta} close to the surface is anticipated to be effective in manipulating the surface property and enhancing the OER performance of the Fe-doped Ta_2O_5 system.

To evaluate the OER catalytic activity of the (200) surface of Fe-doped Ta_2O_5, four elementary steps of the OER process with intermediates of HO*, O*, and HOO* are considered as seen in Fig. 4(a).[12,30] Each elementary step is associated with a free-energy change of ΔG_{1-4}, in which the largest ΔG limits the overall OER activity called potential limiting step (PLS). Therefore, the calculated onset overpotential can be obtained by the formula $\eta = \max\ [\Delta G_1,\ \Delta G_2,\ \Delta G_3,\ \Delta G_4] - 1.23$ (V), where the 1.23 V refers to the equilibrium potential of oxygen evolution for standard hydrogen electrode. The η represents the overpotential required by thermodynamics to start OER and serves as the key descriptor for evaluating OER activity. The binding strength between the intermediates and catalyst's surface largely determines the η value.[30] Please refer to our previous work for detailed evaluation method of OER catalytic activity via first-principles approach.[12] Our previous study shows that only one oxygen site on (200) surface of pure Ta_2O_5 is active in OER catalysis.[12] There is another inert oxygen site on pure (200) surface possessing a high calculated onset overpotential of 0.65 V with PLS of O* to HOO*. Thus, activating the inert oxygen site toward OER catalysis is critical for further enhancing the OER activity. Interestingly, when an Fe_{Ta} substitutional dopant is incorporated and connected to the surface oxygen site, the calculated onset overpotential drops to as low as 0.21 V with PLS of HO* to O* as shown by the free-energy diagrams in Fig. 4(b). It can be seen that when an electrode potential of $U \geq 1.44$ V is applied, OER will take place continuously on the surface because of the all-negative free-energy changes (green diagram). Therefore, the Fe_{Ta} dopant generates a new active oxygen site toward OER on (200) surface of Ta_2O_5, enhancing the OER activity. The decrease in calculated onset overpotential induced by the surface Fe_{Ta} dopant might be due to the electron transfer between Fe_{Ta} dopant and the coordinated oxygens. The calculated onset overpotential (0.21 V)

https://doi.org/10.1557/mrc.2017.55 Published online by Cambridge University Press

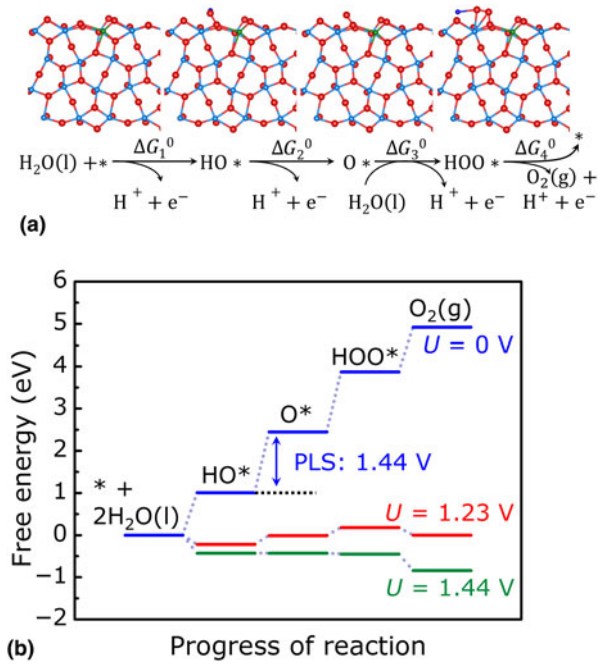


Figure 4. (a) Progress of reaction for OER with intermediates HO*, O*, and HOO* on top of an oxygen site on the (200) surface of Fe-doped Ta_2O_5 in Fig. 3(c). (b) Standard free-energy diagrams for the OER at different electrode potentials U of 0, 1.23, and 1.44 V.

agrees well with the experimental value (0.22 V).[24,30] It suggests that the Fe-doped Ta_2O_5 can be another economical and efficient OER catalytic system for future clean energy applications.

Apart from the amount of active OER sites, electronic conductivity of the catalyst also strongly affects the experimental overpotential.[11,20] The active OER sites on catalytic surface shall be electrically connected to the conductive electrode, which requires efficient charge transfer over the catalyst and the electrode. Therefore, conductive catalysts of metallic behavior are the most favorable. Unfortunately, Ta_2O_5 is a well-known insulator with a large bandgap, which is intrinsically poor in electron transfer. To meet the challenge, Fe_{Ta} dopant can be used to tune the electronic property of Ta_2O_5 matrix by introducing additional energy states in bandgap. The DOS plot of pure Ta_2O_5 in Fig. S4(a) (Supplementary material) shows a large calculated bandgap of 3.8 eV indicating the insulating behavior of the Ta_2O_5 matrix. Notably, after doping Fe_{Ta}, dense energy states appear within the bandgap and near the Fermi level, making the bandgap vanish. It suggests that Fe_{Ta} dopants can increase the conductivity of the Ta_2O_5 matrix and accelerate the electron transfer. Furthermore, the projected density of states (PDOS) plot of Fe, O, and Ta of Fe-doped Ta_2O_5 in Fig. S4(b) (Supplementary material) demonstrates that the energy states near the Fermi level are dominated by oxygen. It is also confirmed by the partial charge density in Fig. S4(c) (Supplementary material) that the charges near the Fermi level are mainly distributed around the oxygens in connection with Fe_{Ta}. It can be attributed to the Fe 3*d*–O 2*p* hybridization agreeing well with the XPS analysis (Fig. 1(d) and Supplementary material: Fig. S3). Thus, we argue that the Fe_{Ta} dopants can promote rapid electron transfer over oxygens. It is recalled that an oxygen site on surface is identified as the active OER site in Fe-doped Ta_2O_5 [Fig. 4(a)]. Therefore, the accelerated electron transfer over oxygens induced by Fe_{Ta} dopants can effectively reduce the overpotential and benefit the OER catalytic performance of the Fe-doped Ta_2O_5 system.

Conclusions

In summary, we report Fe-doped Ta_2O_5 to be an economical catalytic system toward efficient OER via a combined experimental and first-principles study. Fe dopants (5 at.%) can enhance the OER current density of Ta_2O_5 nanolayer by as large as ~47% from 74 to 109 mA/cm^2 at an overpotential of 0.5 V. The 5 at.% Fe-doped Ta_2O_5 catalyst has a low onset overpotential of 0.22 V, an overpotential of 0.38 V at 10 mA/cm^2 and a small Tafel slope of 54 mV/dec, which serves as a promising candidate to replace the precious Ru- and Ir-based catalysts. Furthermore, first-principles simulation demonstrates that substitutional Fe_{Ta} dopants favor to form on Ta_2O_5 surface, which generate a new active OER site on surface and hence directly enhance the OER activity. Meanwhile, the Fe_{Ta} dopants are able to reduce the bandgap of Ta_2O_5 and accelerate the electron transfer over oxygens, benefiting the OER catalytic performance. Our development and understanding of the Fe-doped Ta_2O_5 system extend the applications of the earth-abundant Fe element in transition metal oxides for enhancing the OER efficiency and open up new opportunity of designing economical OER catalysts for renewable energy technologies.

Supplementary material

The supplementary material for this article can be found at https://doi.org/10.1557/mrc.2017.55

Acknowledgments

A. L. would like to acknowledge the financial support from Natural Science Foundation of Hubei Province (Grant no. 2013CFC104). J. D. is grateful for the financial support from the National Research Foundation (NRF-CRP16-2015-01) and NUS Strategic Fund (R261-509-001-646). W. X. performs the first-principles calculations.

References

1. M.S. Dresselhaus and I.L. Thomas: Alternative energy technologies. *Nature* **414**, 332 (2001).
2. J.H. Montoya, L.C. Seitz, P. Chakthranont, A. Vojvodic, T.F. Jaramillo, and J. K. Norskov: Materials for solar fuels and chemicals. *Nat. Mater.* **16**, 70 (2017).
3. S. Hoang and P.-X. Gao: Nanowire array structures for photocatalytic energy conversion and utilization: a review of design concepts, assembly and integration, and function enabling. *Adv. Energy Mater.* **6**, 1600683 (2016).
4. C. Liu, R. Roder, L. Zhang, Z. Ren, H. Chen, Z. Zhang, C. Ronning, and P.-X. Gao: Highly efficient visible-light driven photocatalysts: a case of

https://doi.org/10.1557/mrc.2017.55 Published online by Cambridge University Press

zinc stannate based nanocrystal assemblies. *J. Mater. Chem. A* **2**, 4157 (2014).
5. B. Weng, F. Xu, C. Wang, W. Meng, C.R. Grice, and Y. Yan: A layered $Na_{1-x}Ni_yFe_{1-y}O_2$ double oxide oxygen evolution reaction electrocatalyst for highly efficient water-splitting. *Energy Environ. Sci.* **10**, 121 (2017).
6. X. Xu, F. Song, and X. Hu: A nickel iron diselenide-derived efficient oxygen-evolution catalyst. *Nat. Commun.* **7**, 12324 (2016).
7. Y. Qiu, L. Xin, and W. Li: Electrocatalytic oxygen evolution over supported small amorphous Ni–Fe nanoparticles in alkaline electrolyte. *Langmuir* **30**, 7893 (2014).
8. W. Song, Z. Ren, S.-Y. Chen, Y. Meng, S. Biswas, P. Nandi, H.A. Elsen, P.-X. Gao, and S.L. Suib: Ni- and Mn-promoted mesoporous Co_3O_4: a stable bifunctional catalyst with surface-structure-dependent activity for oxygen reduction reaction and oxygen evolution reaction. *ACS Appl. Mater. Interfaces* **8**, 20802 (2016).
9. D. Gao, J. Zhang, T. Wang, W. Xiao, K. Tao, D. Xue, and J. Ding: Metallic Ni_3N nanosheets with exposed active surface sites for efficient hydrogen evolution. *J. Mater. Chem. A* **4**, 17363 (2016).
10. X. Huang, M. Leng, W. Xiao, M. Li, J. Ding, T.L. Tan, W.S.V. Lee, and J. Xue: Activating basal planes and S-terminated edges of MoS_2 toward more efficient hydrogen evolution. *Adv. Funct. Mater.* **27**, 1604943 (2017).
11. W. Xiao, P. Liu, J. Zhang, W. Song, Y.P. Feng, D. Gao, and J. Ding: Dual-functional N dopants in edges and basal plane of MoS_2 nanosheets toward efficient and durable hydrogen evolution. *Adv. Energy Mater.* **7**, 1602086 (2017).
12. W. Xiao, X. Huang, W. Song, Y. Yang, T.S. Herng, J.M. Xue, Y.P. Feng, and J. Ding: High catalytic activity of oxygen-induced (200) surface of Ta_2O_5 nanolayer towards durable oxygen evolution reaction. *Nano Energy* **25**, 60 (2016).
13. L. Wang, X. Huang, and J. Xue: Graphitic mesoporous carbon loaded with iron–nickel hydroxide for superior oxygen evolution reactivity. *ChemSusChem* **9**, 1835 (2016).
14. Y. Li, M. Gong, Y. Liang, J. Feng, J.-E. Kim, H. Wang, G. Hong, B. Zhang, and H. Dai: Advanced zinc-air batteries based on high-performance hybrid electrocatalysts. *Nat. Commun.* **4**, 1805 (2013).
15. S. Dresp, F. Luo, R. Schmack, S. Kuhl, M. Gliech, and P. Strasser: An efficient bifunctional two-component catalyst for oxygen reduction and oxygen evolution in reversible fuel cells, electrolyzers and rechargeable air electrodes. *Energy Environ. Sci.* **9**, 2020 (2016).
16. S. Trasatti: Electrocatalysis in the anodic evolution of oxygen and chlorine. *Electrochim. Acta* **29**, 1503 (1984).
17. S. Cherevko, T. Reier, A.R. Zeradjanin, Z. Pawolek, P. Strasser, and K.J. J. Mayrhofer: Stability of nanostructured iridium oxide electrocatalysts during oxygen evolution reaction in acidic environment. *Electrochem. Commun.* **48**, 81 (2014).
18. Y. Yamashita, M. Tada, M. Kakihana, M. Osada, and K. Yoshida: Synthesis of RuO_2-loaded $BaTi_nO_{2n+1}$ ($n = 1$, 2 and 5) using a polymerizable complex method and its photocatalytic activity for the decomposition of water. *J. Mater. Chem.* **12**, 1782 (2002).
19. S. Morales and A. Fernandez: Unsupported $Pt_xRu_yIr_z$ and Pt_xIr_y as bi-functional catalyst for oxygen reduction and oxygen evolution reactions in acid media, for unitized regenerative fuel cell. *Int. J. Electrochem. Sci.* **8**, 12692 (2013).
20. M.S. Burke, L.J. Enman, A.S. Batchellor, S. Zou, and S.W. Boettcher: Oxygen evolution reaction electrocatalysis on transition metal oxides and (oxy)hydroxides: activity trends and design principles. *Chem. Mater.* **27**, 7549 (2015).
21. R. Subbaraman, D. Tripkovic, K.-C. Chang, D. Strmcnik, A.P. Paulikas, P. Hirunsit, M. Chan, J. Greeley, V. Stamenkovic, and N.M. Markovic: Trends in activity for the water electrolyser reactions on 3d M(Ni,Co,Fe, Mn) hydr(oxy)oxide catalysts. *Nat. Mater.* **11**, 550 (2012).
22. C.C.L. McCrory, S. Jung, J.C. Peters, and T.F. Jaramillo: Benchmarking heterogeneous electrocatalysts for the oxygen evolution reaction. *J. Am. Chem. Soc.* **135**, 16977 (2013).
23. M.S. Burke, M.G. Kast, L. Trotochaud, A.M. Smith, and S.W. Boettcher: Cobalt–iron (oxy)hydroxide oxygen evolution electrocatalysts: the role of structure and composition on activity, stability, and mechanism. *J. Am. Chem. Soc.* **137**, 3638 (2015).
24. D. Friebel, M.W. Louie, M. Bajdich, K.E. Sanwald, Y. Cai, A.M. Wise, M.-J. Cheng, D. Sokaras, T.-C. Weng, R. Alonso-Mori, R.C. Davis, J. R. Bargar, J.K. Nørskov, A. Nilsson, and A.T. Bell: Identification of highly active Fe sites in (Ni,Fe)OOH for electrocatalytic water splitting. *J. Am. Chem. Soc.* **137**, 1305 (2015).
25. M. Görlin, P. Chernev, J. Ferreira de Araújo, T. Reier, S. Dresp, B. Paul, R. Krähnert, H. Dau, and P. Strasser: Oxygen evolution reaction dynamics, Faradaic charge efficiency, and the active metal redox states of Ni–Fe oxide water splitting electrocatalysts. *J. Am. Chem. Soc.* **138**, 5603 (2016).
26. S. Zou, M.S. Burke, M.G. Kast, J. Fan, N. Danilovic, and S.W. Boettcher: Fe (oxy)hydroxide oxygen evolution reaction electrocatalysis: intrinsic activity and the roles of electrical conductivity, substrate, and dissolution. *Chem. Mater.* **27**, 8011 (2015).
27. E. Atanassova: Thin RF sputtered and thermal Ta_2O_5 on Si for high density DRAM application. *Microelectron. Reliab.* **39**, 1185 (1999).
28. T. Fujii, F.M.F. de Groot, G.A. Sawatzky, F.C. Voogt, T. Hibma, and K. Okada: *In situ* XPS analysis of various iron oxide films grown by NO_2-assisted molecular-beam epitaxy. *Phys. Rev. B* **59**, 3195 (1999).
29. S.-H. Lee, J. Kim, S.-J. Kim, S. Kim, and G.-S. Park: Hidden structural order in orthorhombic Ta_2O_5. *Phys. Rev. Lett.* **110**, 235502 (2013).
30. I.C. Man, H.-Y. Su, F. Calle-Vallejo, H.A. Hansen, J.I. Martínez, N. G. Inoglu, J. Kitchin, T.F. Jaramillo, J.K. Nørskov, and J. Rossmeisl: Universality in oxygen evolution electrocatalysis on oxide surfaces. *ChemCatChem* **3**, 1159 (2011).

https://doi.org/10.1557/mrc.2017.55 Published online by Cambridge University Press